MODELLING AND OPTIMIZATION OF HEXAVALENT CHROMIUM [CR (VI)] REMOVAL FROM AQUEOUS SOLUTION USING MODIFIED AND NON-MODIFIED RICE HUSK: INTEGRATED RESPONSE SURFACE METHODOLOGY AND ARTIFICIAL NEURAL APPROACHES

***Ije, I.[1], Ezugwu, C. N.[2], Mmonwuba, N. C.[3], Eze, E. E.[4], Eboh, S.[5], and Emeka-Chris C. C.[6]**

[1,4,5]Department of Civil Engineering, Michael Okpara University of Agriculture, Umudike
[2]Department of Civil Engineering, Alex Ekwueme Federal University, Ndufu-Alike, Ikwo LGA, Ebonyi State.
[3]Department of Civil Engineering Chukwuemeka Odumegwu Ojukwu University, Uli Campus, Anambra State
[6]Department of Agricultural and Biosystems Engineering, Michael Okpara University of Agriculture, Umudike

*Corresponding author: ije.innocent@mouau.edu.ng

ABSTRACT

Hexavalent chromium [Cr(VI)] in industrial wastewater requires treatment methods that are efficient, affordable and adaptable to resource-constrained settings. This study compared nitric-acid-modified and non-modified rice husk in a 29-run response surface design comprising initial chromium concentration (20-100 mg/L), pH (2-10), adsorbent dose (0.10-1.00 g) and contact time (10-70 min). Residual dissolved chromium and percentage removal were modelled with quadratic response surface methodology (RSM) and a 4-10-1 artificial neural network (ANN). Chemical modification lowered the mean residual concentration from 34.26 to 20.59 mg/L and increased mean removal from 45.66% to 67.00%, a gain of 21.33 percentage points. The maximum experimental removal was 98.2% for modified rice husk. At the replicated centre point, modified and non-modified materials produced 68.77 ± 0.31% and 44.10 ± 0.17% removal, respectively (n = 3). For modified rice husk, the RSM calibration yielded R^2 = 0.9940 and RMSE = 1.3923 mg/L, while leave-one-out cross-validation yielded R^2cv = 0.9701 and RMSEcv = 3.1111 mg/L. The corresponding ANN calibration/split metrics were R^2 = 0.9292 and RMSE = 4.7909 mg/L. Solution pH was the dominant factor, followed by initial concentration, and the concentration-pH interaction was highly significant. Constrained optimization located the best model-based operating region at pH 2.0, 100 mg/L, 1.00 g and 70 min. The results demonstrate that nitric-acid modification improves rice-husk performance and that RSM offers reliable interpolation within the investigated domain, although validation with real wastewater, chromium-speciation analysis, regeneration testing and continuous-flow trials remains necessary.

Keywords: Adsorption; artificial neural network; Cr(VI); rice husk; response surface methodology; wastewater treatment

Nomenclature

Symbol/term	Meaning
A	Initial Cr(VI) concentration (mg/L)
B	Solution pH
C	Adsorbent dosage (g)
D	Contact time (min)
C0	Initial Cr(VI) concentration (mg/L)
Ce	Residual dissolved chromium concentration after treatment (mg/L)
RSM	Response surface methodology
ANN	Artificial neural network
RMSE	Root mean squared error
MAE	Mean absolute error
ARE	Average relative error
LOOCV	Leave-one-out cross-validation
MDL	Method detection limit
LOQ	Limit of quantification

1.0 INTRODUCTION

Chromium-bearing effluents arise from electroplating, leather processing, metal finishing, mining, pigment manufacture and related industrial activities. In water, chromium occurs mainly as Cr(III) and Cr(VI); the hexavalent form is generally more mobile and toxic because it occurs as soluble oxyanions. Consequently, treatment systems must reduce the dissolved chromium burden before discharge or reuse. Available technologies include chemical reduction-precipitation, adsorption, ion exchange, membrane separation and electrochemical treatment. Each can be effective, but cost, chemical consumption, energy demand, sludge generation and operational complexity often limit deployment at small or decentralized facilities (Moussavi & Barikbin, 2010; Ren *et al*., 2020; Wu *et al*., 2024).

Adsorption using agricultural residues is attractive because it can valorise locally available biomass while providing a relatively simple treatment step. Rice husk contains lignocellulosic carbon, silica and oxygen-containing surface groups that can interact with chromate and dichromate species. Earlier work established the feasibility of rice-husk sorbents (Bansal *et al*., 2009), and recent studies have reported 96.8% removal with rice-husk biochar, 97% removal with amide-modified rice-husk biochar, and improved performance after incorporation of MgO or iron-bearing phases (Khalil *et al*., 2020; Ali *et al*., 2023; Mustapha *et al*., 2024; Liu *et al*., 2025). These studies also show that adsorption performance depends strongly on pH, surface chemistry, dose, contact time and influent concentration Chemical treatment can remove mineral impurities, increase surface roughness and expose or introduce functional groups, but the benefit must be quantified against the additional acid demand, washing requirement and spent-sorbent management (Ngah & Hanafiah, 2008). Nitric acid was selected in the present work to compare a reproducibly modified rice-husk material with its non-modified counterpart. The comparison is important because percentage removal alone may obscure differences in residual concentration, robustness across operating conditions and the practical cost of chemical activation.

Multivariable modelling can reduce the number of experiments needed to quantify interacting process factors. RSM provides interpretable polynomial effects, ANOVA and constrained optimization, whereas ANN models can capture nonlinear patterns without assuming a fixed equation. Recent Cr(VI) studies have used both approaches, but their relative performance is dataset-dependent: RSM has provided accurate, transparent fits in some adsorption systems, while ANN has performed better in other batch and column studies (Mahmoud *et al*., 2021; Vinayagam *et al*., 2022; Ren *et al*., 2025). Small experimental datasets therefore require explicit validation rather than reliance on calibration statistics alone.

The novelty of this study is the side-by-side evaluation of nitric-acid-modified and non-modified rice husk under the same 29-run four-factor design, coupled with RSM, ANN, residual diagnostics, leave-one-out cross-validation, sensitivity analysis, sweet-spot identification and technology benchmarking. This integrated framework quantifies the performance gain caused by modification, identifies the controlling factor interactions, tests model generalization and places the proposed adsorbent in the context of recent adsorption and conventional Cr(VI) treatment technologies. The study therefore advances beyond a single-adsorbent optimization by linking comparative material performance, predictive reliability and scale-up constraints in one analysis.

2.0 MATERIALS AND METHODS

Figure 1 summarizes the experimental, characterization, modelling and optimization workflow used in this study.

2.1. Materials and chemical reagents

Rice husk was collected in Afikpo, Ebonyi State, Nigeria, and used as the precursor biomass. Analytical-grade potassium dichromate ($K_2Cr_2O_7$) was used to prepare synthetic chromium solutions. Hydrochloric acid (HCl) and sodium hydroxide (NaOH), each at 1.0 mol/L, were used for pH adjustment. Analytical-grade nitric acid (HNO_3) was used for surface modification, and deionized water was used for washing, solution preparation and dilution.

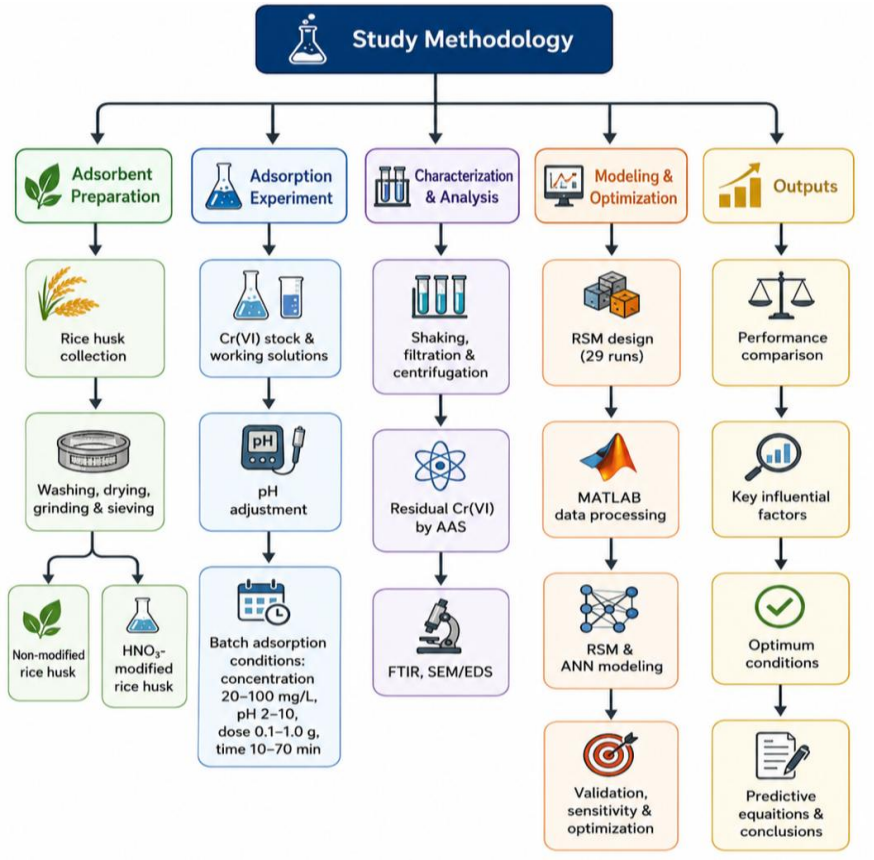

Figure 1: Study workflow from adsorbent preparation to modeling and optimization.

2.2. Preparation of modified and non-modified rice husk adsorbents

The collected rice husk was cut to approximately 2 cm, screened and washed with deionized water to remove adhering dirt and soluble impurities. The material was oven-dried at 105 °C for 6 h, ground, and sieved to a particle size of 150-250 µm. It was then carbonized in a muffle furnace (SXL, Searchtech) at 350 °C for 2 h. A portion of the carbonized material was retained as the non-modified adsorbent. For modification, 1.0 g of carbonized rice husk was contacted with 20 mL of 1.0 mol/L HNO_3 and agitated at 120 rpm for 2 h at 60 ± 2 °C. The solid was separated, washed repeatedly with deionized water until the final wash reached pH 7.0 ± 0.2, oven-dried at 150 °C to constant mass for at least 2 h, cooled in a desiccator and stored in airtight containers. Table 1 summarizes the preparation conditions, and Figure 2 shows the batch-treatment sequence.

Table 1: Adsorbent preparation conditions.

Protocol item	**Condition**	**Purpose/control**
Modifying reagent	Analytical-grade HNO_3	Acid activation of carbonized rice husk
Acid concentration	1.0 mol/L	Standardized modification strength
Solid-to-liquid ratio	1 g dry adsorbent per 20 mL acid	Uniform wetting and contact
Treatment	2 h at 60 ± 2 °C and 120 rpm	Controlled reaction time, temperature and mixing
Washing endpoint	Deionized water to pH 7.0 ± 0.2	Removal of residual acid and soluble products

Protocol item	Condition	Purpose/control
Drying/storage	150 °C to constant mass; desiccator; airtight container	Stable dry mass and reduced moisture uptake

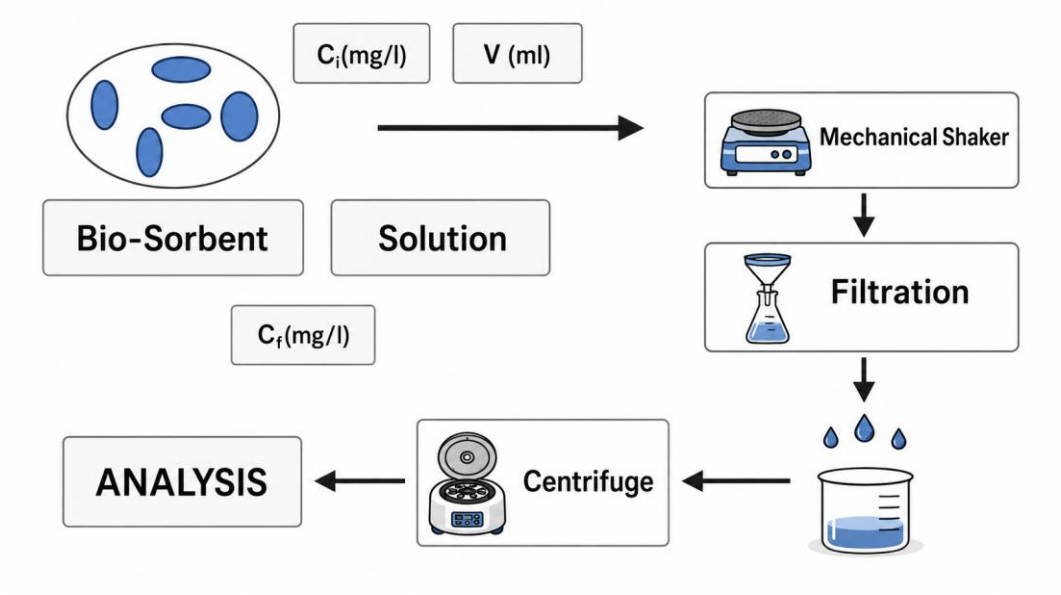

Figure 2: Batch adsorption workflow for treatment and residual chromium analysis.

2.3. Preparation of stock and working solutions

A 1000 mg/L stock solution expressed as chromium was prepared by dissolving 2.829 g of $K_2Cr_2O_7$ in deionized water and diluting to 1.000 L. Working solutions of 20, 60 and 100 mg/L were prepared by volumetric dilution. The solution pH was adjusted to 2, 6 or 10 with 1.0 mol/L HCl or NaOH and measured with a calibrated pH meter (pH-10, serial no. 1218). The principal dissolution, acid-base and surface-interaction steps relevant to the synthetic system are represented by Reactions (R1)-(R8).

$$K_2Cr_2O_7(s) \rightarrow 2K^+(aq) + Cr_2O_7^{2-}(aq) \quad (R1)$$

$$Cr_2O_7^{2-}(aq) + H_2O(l) \rightleftharpoons 2HCrO_4^-(aq) \quad (R2)$$

$$HCrO_4^-(aq) \rightleftharpoons CrO_4^{2-}(aq) + H^+(aq) \quad (R3)$$

$$HCl(aq) \rightarrow H^+(aq) + Cl^-(aq) \quad (R4)$$

$$NaOH(aq) \rightarrow Na^+(aq) + OH^-(aq) \quad (R5)$$

$$H^+(aq) + OH^-(aq) \rightarrow H_2O(l) \quad (R6)$$

$$\equiv SOH + H^+ \rightleftharpoons \equiv SOH_2^+ \quad (R7)$$

$$\equiv SOH_2^+ + HCrO_4^- \rightleftharpoons \equiv SOH_2^+ \cdots HCrO_4^- \quad (R8)$$

At low pH, protonation of surface sites (R7) favours electrostatic attraction of hydrogen chromate and dichromate anions (R8). Lignocellulosic carbon may also promote partial Cr(VI)-to-Cr(III) reduction; because the oxidation state was not measured directly, this pathway is treated as plausible rather than experimentally confirmed.

2.4. Batch adsorption procedure

Adsorbent doses of 0.10, 0.55 and 1.00 g were added to labelled conical flasks containing chromium solutions at the prescribed initial concentration and pH. The suspensions were agitated on a multipurpose mechanical shaker (HY-2, Searchtech) at 120 rpm for 10, 40 or 70 min. After contact, samples were filtered, transferred to centrifuge tubes and centrifuged at 3000 rpm for 5 min (80-2 centrifuge). A 10 mL aliquot of clarified supernatant was analyzed by atomic absorption spectrophotometry (AAS; UNICO 1100).

Dissolved chromium was measured at 357.9 nm in air-acetylene flame mode. Calibration standards covered 0.5-10.0 mg/L, and samples above this range were diluted before measurement. Calibration was accepted at $R^2 \geq 0.995$. Quality control comprised reagent and calibration blanks, duplicate analysis, continuing calibration verification after every ten samples and matrix-spike recovery with a target range of 90-110%. The method detection limit and reporting limit were 0.01 and 0.03 mg/L, respectively. AAS is element-specific but not oxidation-state-specific; therefore, the measured response represents dissolved total chromium and is used here as an operational proxy for residual Cr(VI) in the synthetic system. Direct Cr(VI) speciation by the 1,5-diphenylcarbazide method or ion chromatography is required in future work to distinguish adsorption from reduction.

2.5. Experimental design and response variables

The experiments followed a 29-run response surface design with four factors: initial chromium concentration (20, 60 and 100 mg/L), pH (2, 6 and 10), adsorbent dose (0.10, 0.55 and 1.00 g) and contact time (10, 40 and 70 min). Three centre-point runs at 60 mg/L, pH 6.0, 0.55 g and 40 min were included to estimate pure error and assess repeatability. Responses were residual dissolved chromium concentration and percentage removal for modified and non-modified rice husk.

The centre-point triplicates were summarized by mean, standard deviation and coefficient of variation. Non-centre design points were single observations; their uncertainty was therefore evaluated through model residuals and cross-validation rather than assigned replicate standard deviations. RSM models used all 29 runs. To provide an internal test independent of calibration, leave-one-out cross-validation (LOOCV) was applied to each RSM model, with one run withheld in turn and predicted from a model fitted to the remaining 28 runs.

2.6. Characterization and analytical conditions

Fourier transform infrared (FTIR) spectra were acquired in attenuated total reflectance mode over 4000-400 cm^{-1} at 4 cm^{-1} resolution using 32 scans per sample and background correction before each run. Scanning electron microscopy (SEM) was used to compare surface morphology before and after adsorption; samples were mounted on carbon tabs, sputter-coated where required, and imaged at 15 kV with scale-bar-supported magnification. Energy-dispersive X-ray spectroscopy (EDS) was acquired in the SEM chamber at 15 kV with an approximately 60 s live time and standardless ZAF/Φ(ρz)-type quantification. Because EDS is semiquantitative and sensitive to the selected field, coating and substrate, elemental results were used for exploratory interpretation rather than mass-balance confirmation. The instrumental conditions and quality-control criteria are summarized in Table 2.

Table 2: Instrumental operating conditions and quality controls.

Instrument/method	Operating conditions	QA/QC and acceptance criteria
FTIR	ATR-FTIR; 4000-400 cm−1 spectral range; 4 cm−1 resolution; 32 scans per sample; background correction before each run.	Baseline correction applied before peak assignment; major bands reported with wavenumber and functional-group interpretation.
SEM	Samples mounted on carbon tape and sputter-coated where necessary; imaging at 15 kV with scale-bar-supported magnifications and 8-10 mm working distance.	Representative fields selected before and after adsorption to describe surface roughness, porosity and post-treatment morphology.
EDS	EDS acquired in SEM chamber at 15 kV; approximately 60 s live time; standardless ZAF/Φ(ρz)-type quantification; results reported as atomic and weight percentages.	At least three representative points/areas should be checked where possible; elemental totals and unusual elements should be interpreted cautiously.
AAS for dissolved chromium	UNICO 1100; air-acetylene flame; Cr hollow-cathode lamp; 357.9 nm; calibration range 0.5-10.0 mg/L; dilution for samples above range.	Calibration $R^2 \geq 0.995$; MDL 0.01 mg/L; reporting limit 0.03 mg/L; blanks, duplicates, continuing calibration verification and 90-110% spike recovery. AAS does not distinguish Cr(VI) from Cr(III).

2.7. Computational modeling framework

The dataset was processed in MATLAB R2024a. The input matrix contained initial concentration (A), pH (B), dose (C) and contact time (D), while separate response vectors contained the residual concentrations for modified and non-modified rice husk. Data were checked for missing values, range errors and duplicated design settings before fitting, diagnostic analysis, cross-validation and optimization.

2.7.1. Response surface methodology

A full second-order polynomial was fitted to each response according to Equation (1):

$$Y = \beta^0 + \Sigma_i \beta_i X_i + \Sigma_i < {}_j \beta_{ij} X_i X_j + \Sigma_i \beta_{ii} X_i{}^2 \quad (1)$$

where Y is the predicted residual concentration; X_i and X_j are process variables; and β_o, β_i, β_{ij} and β_{ii} are the intercept, linear, interaction and quadratic coefficients, respectively. Model adequacy was evaluated by ANOVA, coefficient significance, residual plots, lack-of-fit testing and LOOCV. The coefficient of determination was calculated with Equation (2).

2.7.2. Artificial neural network modelling

The ANN comparator used a 4-10-1 feed-forward architecture with four input neurons, ten hidden neurons and one output neuron. The hidden layer used the tansig activation function, the output layer used purelin, and

training used Levenberg-Marquardt back-propagation. The 29 observations were divided into 70% training, 15% validation and 15% testing subsets. Because this split leaves only four to five observations in each holdout subset, ANN results were interpreted as split-sensitive and were not treated as external validation.

2.7.3. Model evaluation metrics

Model performance was evaluated using R^2, mean squared error (MSE), root mean squared error (RMSE), mean absolute error (MAE) and average relative error (ARE), as defined in Equations (2)-(6) as given by Ozioko and Eze (2025).

$$R^2 = 1 - \left[\frac{\Sigma_i(y_i - \hat{y}_i)^2}{\Sigma_i(y_i - \bar{y})^2}\right] \quad (2)$$

$$MSE = \left(\frac{1}{n}\right)\Sigma_i(y_i - \hat{y}_i)^2 \quad (3)$$

$$RMSE = \sqrt{\left[\left(\frac{1}{n}\right)\Sigma_i(y_i - \hat{y}_i)^2\right]} \quad (4)$$

$$MAE = \left(\frac{1}{n}\right)\Sigma_i|y_i - \hat{y}_i| \quad (5)$$

$$ARE(\%) = \left(\frac{100}{n}\right)\Sigma_i\left|\frac{y_i - \hat{y}_i}{y_i}\right| \quad (6)$$

Where y_i is the observed response, $\hat{y}_i$ is the predicted response, $\bar{y}$ is the observed mean, and n is the number of observations. ARE was interpreted cautiously because relative errors become unstable when observed residual concentrations approach zero.

2.7.4. Optimization, sweet-spot detection and sensitivity analysis

Constrained numerical optimization was used to minimize predicted residual concentration, as expressed in Equation (7), while respecting the experimental bounds.

$$minimize\ f(A,B,C,D) = \hat{Y}residual(A,B,C,D) \quad (7)$$

The constraints were $20 \leq A \leq 100$ mg/L, $2 \leq B \leq 10$, $0.10 \leq C \leq 1.00$ g and $10 \leq D \leq 70$ min. The problem was solved with MATLAB fmincon using sequential quadratic programming. Sweet spots were defined as regions with predicted residual concentration below 2 mg/L and removal above 95%. Local sensitivity at the optimum was calculated by a 5% one-factor perturbation according to Equation (8).

$$S_i = \frac{[f(x_i + 0.05x_i) - f(x_i)]}{0.05x_i} \quad (8)$$

2.8. Removal efficiency and dosage interpolation

Removal efficiency was calculated using Equation (9):

$$\eta(\%) = \left[\frac{C^0 - C_e}{C^0}\right] \times 100 \quad (9)$$

where C_0 is the initial concentration and C_e is the measured residual dissolved chromium concentration. Within a bracketed experimental interval, the adsorbent dose required for a target removal can be estimated by linear interpolation using Equation (10):

$$x = x^1 + \left[\frac{\eta target - \eta^1}{\eta^2 - \eta^1}\right](x^2 - x^1) \quad (10)$$

where x is the estimated dose; x_1 and x_2 are the bracketing doses; and η_1 and η_2 are their corresponding removal efficiencies. This expression is an engineering interpolation and should not be extrapolated beyond the tested dose range.

3.0 RESULTS AND DISCUSSION

3.1. FTIR characterization

The post-adsorption FTIR spectrum (Figure 3) contained bands near 3026.8, 2344.5, 1915.9, 1703.4, 1356.8, 1185.3 and 745.5 cm^{-1}. The band near 1703 cm^{-1} is consistent with carbonyl-containing lignocellulosic structures, while the 1357 and 1185 cm^{-1} regions may include C-O and silica-related vibrations commonly reported for rice-husk materials (Bansal et al., 2009). Bands around 2345 cm^{-1} can also contain atmospheric CO_2 contributions, and the 1916 cm^{-1} feature may include combination or background effects. Because a matched pre-adsorption spectrum with quantified shifts is not shown, the spectrum supports the presence of potential binding groups but does not by itself prove a specific Cr(VI) adsorption mechanism. Future work should report paired spectra and peak-shift statistics.

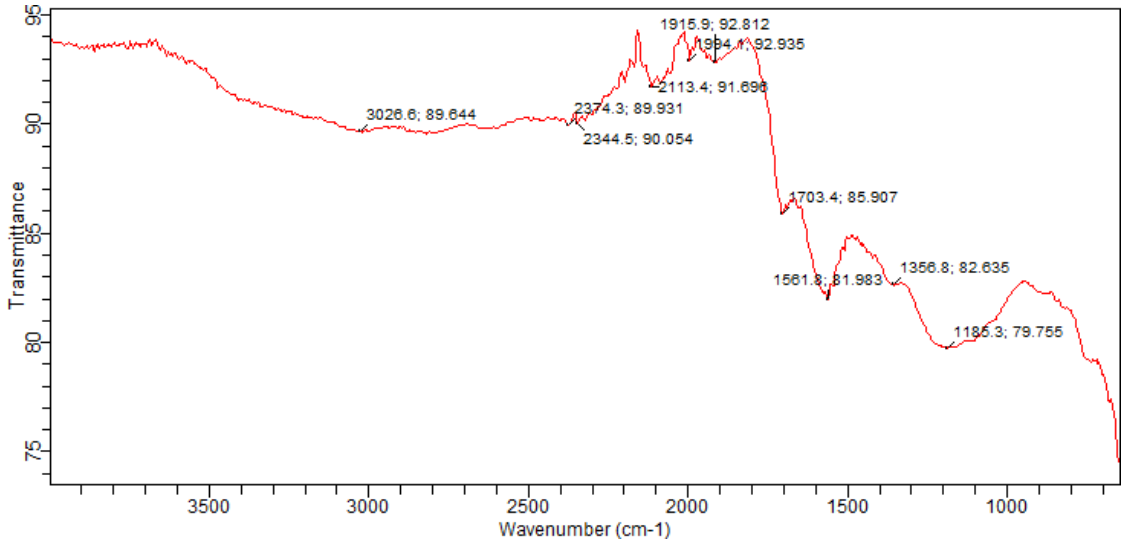

Figure 3: FTIR spectrum of rice husk after Cr(VI) treatment.

3.2. SEM-EDS characterization

Figures 4 and 5 show an irregular, porous and heterogeneous surface before and after treatment. The post-treatment image appears rougher and more fragmented, which is consistent with acid-assisted opening of the lignocellulosic matrix and improved access to surface sites. Similar porous morphologies have been reported for rice-husk-derived adsorbents (Farooque et al., 2009; Khalil et al., 2020). Tables 3 and 4 summarize the associated EDS results. The large changes in Si and C and the presence of Ag, Nb and Y should be interpreted

cautiously because standardless EDS is field-specific and may be affected by the stub, coating, detector background or selected particle. Chromium was not reported in the post-adsorption EDS table; therefore, EDS does not independently confirm chromium uptake in this dataset. Replicating elemental maps or X-ray photoelectron spectroscopy would be required for mechanistic confirmation.

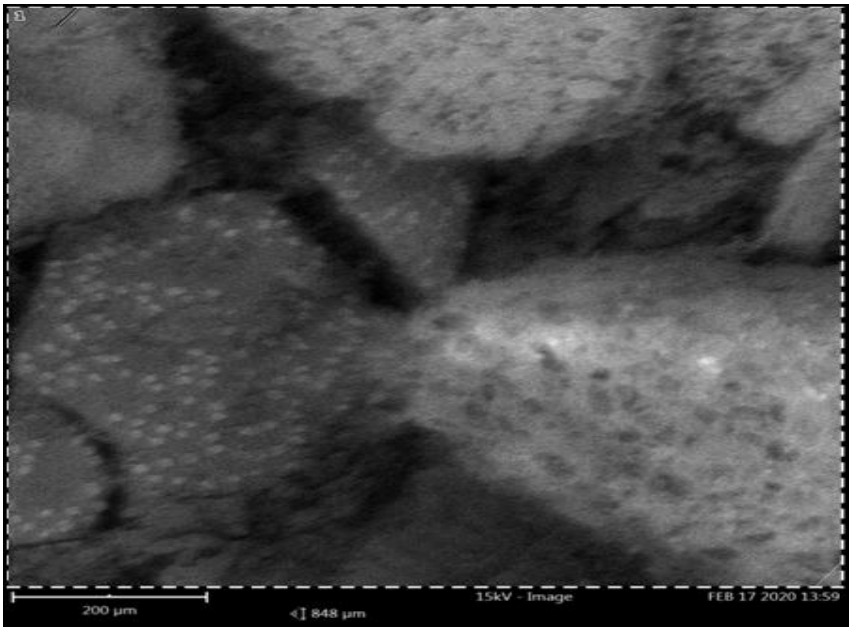

Figure 4: SEM micrograph of rice husk before adsorption.

Table 3: EDS composition of rice husk before adsorption.

Element No.	Symbol	Element	Atomic conc. (%)	Weight conc. (%)
14	Si	Silicon	59.51	55.76
15	P	Phosphorus	7.13	7.37
47	Ag	Silver	1.56	5.62
20	Ca	Calcium	3.2	4.27
6	C	Carbon	10.65	4.27
41	Nb	Niobium	1.22	3.77
19	K	Potassium	2.43	3.17
16	S	Sulfur	2.93	3.14
17	Cl	Chlorine	2.51	2.97
39	Y	Yttrium	0.66	1.96
30	Zn	Zinc	0.79	1.72
13	Al	Aluminium	1.88	1.69
12	Mg	Magnesium	1.86	1.51
8	O	Oxygen	2.16	1.16
26	Fe	Iron	0.57	1.06
11	Na	Sodium	0.45	0.34
7	N	Nitrogen	0.5	0.23
22	Ti	Titanium	0.0	0.0

Table 4: EDS composition of rice husk after adsorption.

Element No.	Symbol	Element	Atomic conc. (%)	Weight conc. (%)
19	K	Potassium	12.96	16.98
6	C	Carbon	41.13	16.56
47	Ag	Silver	3.25	11.74
17	Cl	Chlorine	7.85	9.33
41	Nb	Niobium	2.5	7.8
15	P	Phosphorus	7.14	7.41
20	Ca	Calcium	5.15	6.92
16	S	Sulfur	4.37	4.7
39	Y	Yttrium	1.51	4.51
14	Si	Silicon	3.75	3.53
26	Fe	Iron	1.59	2.97
13	Al	Aluminium	3.23	2.92
11	Na	Sodium	2.46	1.9
12	Mg	Magnesium	1.79	1.46
22	Ti	Titanium	0.53	0.85
8	O	Oxygen	0.8	0.43
7	N	Nitrogen	0.0	0.0

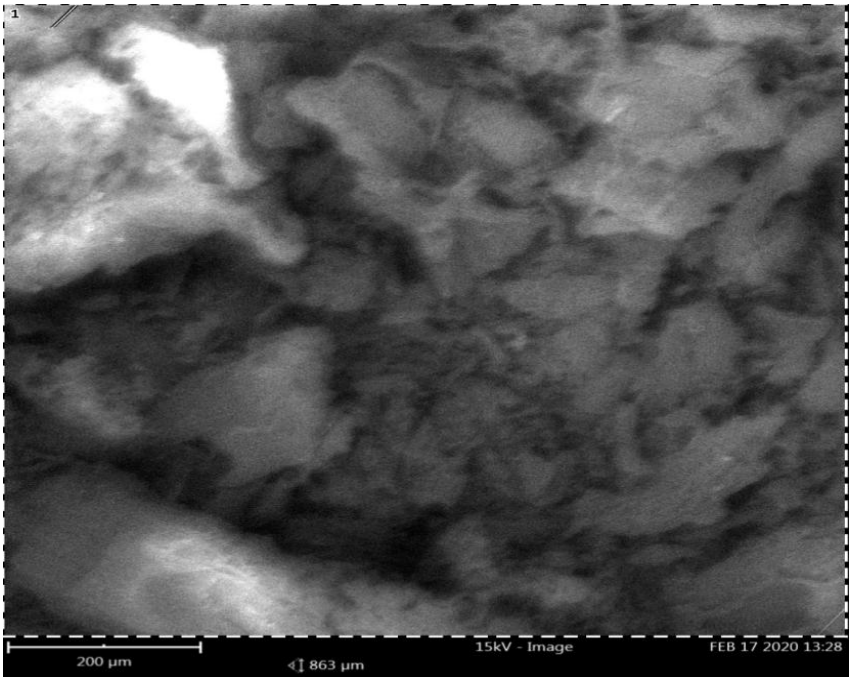

Figure 5: SEM micrograph of rice husk after adsorption.

3.3. Batch adsorption performance

Modified rice husk outperformed the non-modified material across the experimental matrix (Tables 5 and 6). The mean removal increased from 45.66% to 67.00%, equivalent to a gain of 21.33 percentage points or a 46.72% relative improvement. Mean residual concentration decreased from 34.26 to 20.59 mg/L, a 39.90%

reduction. The maximum observed removal was 98.2% for modified rice husk and 86.0% for non-modified rice husk. The improvement is consistent with greater accessibility of protonatable oxygen-containing sites after acid treatment, while the superior performance at low pH agrees with the anionic speciation and surface-protonation mechanism represented by Reactions (R^2), (R7) and (R8).

At the centre point (60 mg/L, pH 6.0, 0.55 g and 40 min), modified rice husk produced 18.74 ± 0.18 mg/L residual concentration and 68.77 ± 0.31% removal, whereas non-modified rice husk produced 33.55 ± 0.10 mg/L and 44.10 ± 0.17% removal (n = 3). The coefficients of variation were approximately 0.95% and 0.30% for the modified and non-modified residual responses, respectively, indicating good repeatability at the design centre. Non-centre runs were not replicated and are therefore presented without inferred standard deviations.

Table 5: Descriptive performance across the 29 experimental runs.

Metric	**Mean**	**Minimum**	**Maximum**
Modified residual concentration (mg/L)	20.59	0.58	68.80
Non-modified residual concentration (mg/L)	34.26	2.80	89.50
Modified removal efficiency (%)	67.00	14.20	98.20
Non-modified removal efficiency (%)	45.66	4.70	86.00
Mean removal gain of modified rice husk	21.33 percentage points	-	-
Relative improvement over the non-modified adsorbent	46.72%	-	-

Table 6: Experimental design and adsorption results.

Run	**Std**	**Initial conc. (mg/L)**	**pH**	**Dose (g)**	**Time (min)**	**Modified residual (mg/L)**	**Non-modified residual (mg/L)**	**Modified removal (%)**	**Non-modified removal (%)**
1	10	100.00	6.00	0.55	10.00	44.60	68.20	55.4	31.8
2	18	100.00	6.00	0.10	40.00	41.80	64.50	58.2	35.5
3	1	20.00	2.00	0.55	40.00	0.70	4.36	96.5	78.2
4	23	60.00	2.00	0.55	70.00	1.32	12.06	97.8	79.9
5	17	60.00	6.00	0.55	40.00	18.90	33.50	68.5	44.2
6	20	100.00	6.00	1.00	40.00	25.50	48.20	74.5	51.8
7	16	60.00	10.00	1.00	40.00	32.64	48.12	45.6	19.8
8	8	20.00	6.00	1.00	70.00	3.54	8.92	82.3	55.4
9	3	20.00	10.00	0.55	40.00	12.32	16.96	38.4	15.2
10	25	100.00	2.00	0.55	40.00	7.90	29.60	92.1	70.4
11	9	20.00	6.00	0.55	10.00	8.94	13.64	55.3	31.8
12	27	60.00	6.00	0.10	40.00	25.08	38.64	58.2	35.6
13	19	60.00	6.00	1.00	10.00	12.40	26.50	79.3	55.8
14	12	100.00	6.00	0.55	70.00	25.50	51.80	74.5	48.2
15	15	60.00	2.00	1.00	40.00	1.08	11.10	98.2	81.5
16	5	60.00	6.00	0.10	10.00	32.88	46.74	45.2	22.1

Run	Std	Initial conc. (mg/L)	pH	Dose (g)	Time (min)	Modified residual (mg/L)	Non-modified residual (mg/L)	Modified removal (%)	Non-modified removal (%)
17	28	60.00	6.00	0.55	40.00	18.78	33.48	68.7	44.2
18	24	60.00	6.00	1.00	70.00	6.50	16.80	89.2	72.0
19	21	100.00	2.00	0.55	10.00	11.60	34.80	88.4	65.2
20	6	100.00	2.00	1.00	10.00	3.80	16.50	96.2	83.5
21	13	60.00	2.00	0.10	40.00	9.42	22.74	84.3	62.1
22	7	20.00	2.00	1.00	10.00	0.58	2.80	97.1	86.0
23	4	100.00	10.00	0.55	40.00	68.80	89.50	31.2	10.5
24	29	60.00	6.00	0.55	40.00	18.54	33.66	69.1	43.9
25	11	20.00	10.00	0.10	70.00	14.80	18.50	26.0	7.5
26	22	60.00	10.00	0.55	10.00	46.50	54.96	22.5	8.4
27	26	60.00	10.00	0.10	40.00	51.50	57.20	14.2	4.7
28	2	20.00	2.00	0.10	10.00	3.20	7.80	84.0	61.0
29	14	100.00	10.00	1.00	70.00	48.00	82.00	52.0	18.0
Mean						20.59	34.26	67.00	45.66

3.4. Exploratory data analysis

Figure 6 confirms the distributional shift produced by chemical modification: modified rice husk yielded lower residual concentrations and higher removal efficiencies. The correlation panel shows that pH had the strongest positive association with residual concentration, indicating poorer removal as the solution became less acidic. Dose and contact time showed weaker marginal linear correlations, but their influence remained significant in the multivariable model because correlation alone does not capture curvature and interactions.

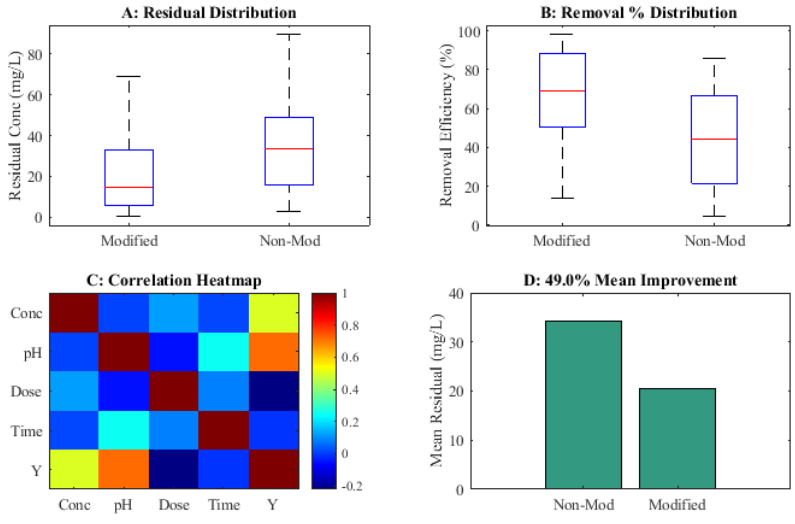

Figure 6: Adsorption distributions, correlations and mean residual improvement.

3.5. RSM ANOVA and factor significance

The full quadratic RSM for modified rice husk was highly significant ($F = 166.15$, $p < 0.0001$; Table 7) and explained 99.40% of the calibration variance (adjusted $R^2 = 0.9880$). pH was the dominant main effect ($F = 1251.20$), followed by initial concentration ($F = 601.03$), dose ($F = 148.76$) and contact time ($F = 63.18$). The concentration-pH interaction was particularly strong ($F = 216.90$), confirming that the effect of pollutant loading depends on acidity. The pH quadratic term was also significant ($p = 0.0006$). The lack-of-fit test was significant ($F = 139.26$, $p = 0.0072$) because the replicated centre point had very small pure error; therefore, the model should be used as an empirical interpolator within the tested domain and judged together with residual diagnostics and LOOCV rather than by R^2 alone.

Table 7: ANOVA for the modified-rice-husk quadratic RSM.

Source	SS	df	MS	F	p-value
Model	9340.23	14	667.16	166.15	<0.0001
A: concentration	2413.36	1	2413.36	601.03	<0.0001
B: pH	5024.01	1	5024.01	1251.20	<0.0001
C: dose	597.32	1	597.32	148.76	<0.0001
D: time	253.70	1	253.70	63.18	<0.0001
AB	870.92	1	870.92	216.90	<0.0001
AC	56.62	1	56.62	14.10	0.0021
AD	67.55	1	67.55	16.82	0.0011
BC	50.08	1	50.08	12.47	0.0033
BD	18.46	1	18.46	4.60	0.0500
CD	23.84	1	23.84	5.94	0.0288
A^2	4.96	1	4.96	1.24	0.2850
B^2	77.90	1	77.90	19.40	0.0006
C^2	0.33	1	0.33	0.08	0.7789
D^2	0.50	1	0.50	0.13	0.7283
Residual	56.22	14	4.02		
Lack of fit	56.15	12	4.68	139.26	0.0072
Pure error	0.067	2	0.034		

3.6. Empirical predictive equations

The fitted models for residual dissolved chromium concentration, expressed in the original factor units, are given by Equations (11) and (12).

$$Ymod = 3.018 + 0.021A - 1.099B - 1.497C + 0.057D + 0.079AB - 0.177AC - 0.003AD - 1.717BC - 0.020BD + 0.163CD + 0.001A^2 + 0.227B^2 + 1.304C^2 - 0.000D^2 \quad (11)$$

$$Ynon-mod = 7.758 + 0.239A - 1.751B - 0.362C - 0.113D + 0.080AB - 0.225AC - 0.002AD + 0.547BC + 0.009BD + 0.123CD + 0.001A^2 + 0.089B^2 - 7.415C^2 - 0.000D^2 \quad (12)$$

Here, A is initial concentration (mg/L), B is pH, C is dose (g), and D is time (min). The equations are intended for interpolation only within 20-100 mg/L, pH 2-10, 0.10-1.00 g and 10-70 min. Negative predicted concentrations are nonphysical polynomial artifacts and must be truncated at zero for engineering interpretation.

3.7. Model diagnostics and Pareto analysis

Residual-versus-predicted and residual-versus-order plots in Figure 7 show no dominant monotonic trend, and the normal-probability plot is approximately linear. These diagnostics support the use of the quadratic model for interpolation, although the significant lack of fit indicates that some local structure remains unresolved. The standardized-effect ranking identifies the concentration-pH interaction and pH curvature among the strongest terms, consistent with chromate speciation and surface protonation. Thus, the diagnostic and ANOVA results converge on pH control as the principal operational requirement.

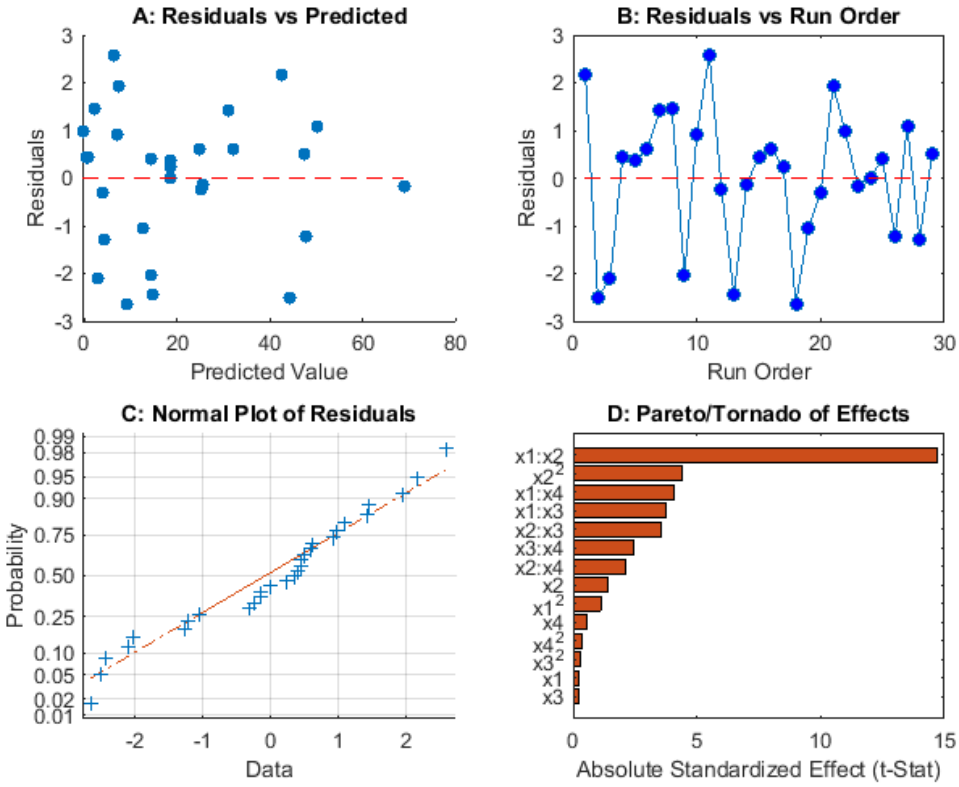

Figure 7: RSM residual diagnostics and standardized-effect ranking.

3.8. Optimization, sweet spot and sensitivity

Constrained optimization located the minimum model response at 100 mg/L initial concentration, pH 2.0, 1.00 g dose and 70 min contact time. The quadratic equation produced a slightly negative residual at this boundary; this is a mathematical artifact and is interpreted as a near-zero residual rather than a physically negative concentration. The sweet-spot contour shows that low pH and high dose provide the broadest region with predicted removal above 95%. Local sensitivity analysis further shows that modest pH increases cause the largest deterioration in performance, whereas time has a smaller incremental effect near the selected upper boundary.

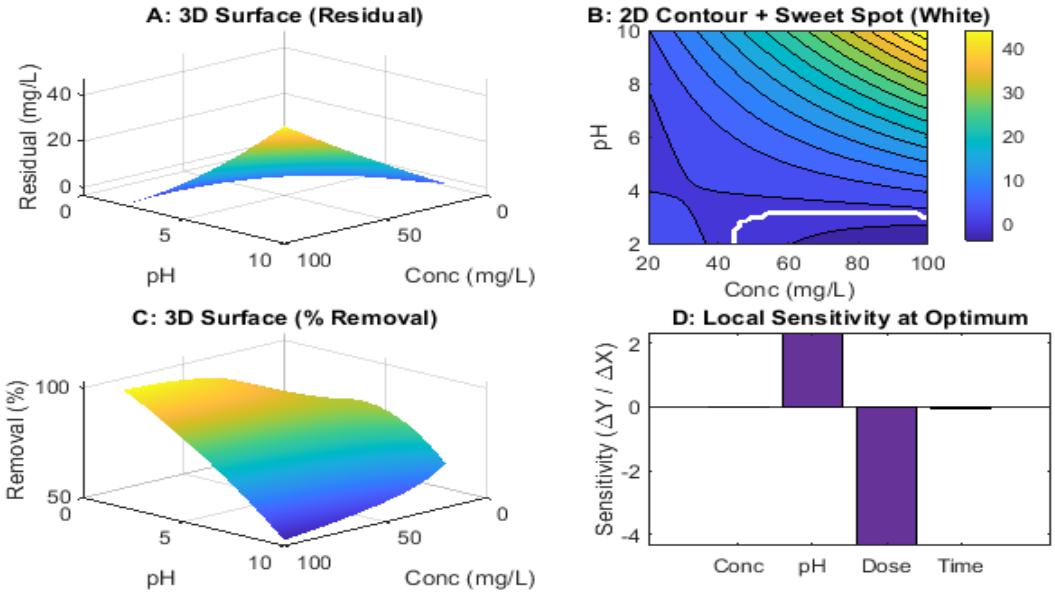

Figure 8: Optimization surfaces, sweet spot and local sensitivity.

3.9. Model performance and internal validation

RSM provided lower calibration errors than ANN for both adsorbent types (Table 8). For modified rice husk, RSM yielded R^2 = 0.9940, RMSE = 1.3923 mg/L and MAE = 1.1132 mg/L, compared with ANN values of 0.9292, 4.7909 and 2.1495 mg/L. For non-modified rice husk, RSM yielded R^2 = 0.9883, RMSE = 2.4807 mg/L and MAE = 1.9057 mg/L, while ANN yielded 0.8725, 8.1977 and 5.4917 mg/L. LOOCV retained strong but lower predictive performance: R^2cv = 0.9701, RMSEcv = 3.1111 mg/L and MAEcv = 2.5342 mg/L for modified rice husk, and R^2cv = 0.9393, RMSEcv = 5.6567 mg/L and MAEcv = 4.4453 mg/L for non-modified rice husk. This validation confirms useful generalization while quantifying the optimism of calibration metrics. The result does not establish universal superiority of RSM; studies with larger datasets have sometimes found ANN more accurate (Vinayagam et al., 2022; Ren et al., 2025). Here, the small sample and split-sensitive ANN holdout likely favoured the more parsimonious polynomial model.

Table 8: Calibration and cross-validation performance.

Model	Adsorbent	Assessment	R^2	RMSE (mg/L)	MAE (mg/L)
RSM	Modified	Calibration	0.9940	1.3923	1.1132
RSM	Modified	LOOCV	0.9701	3.1111	2.5342
ANN	Modified	Reported split	0.9292	4.7909	2.1495
RSM	Non-modified	Calibration	0.9883	2.4807	1.9057
RSM	Non-modified	LOOCV	0.9393	5.6567	4.4453
ANN	Non-modified	Reported split	0.8725	8.1977	5.4917

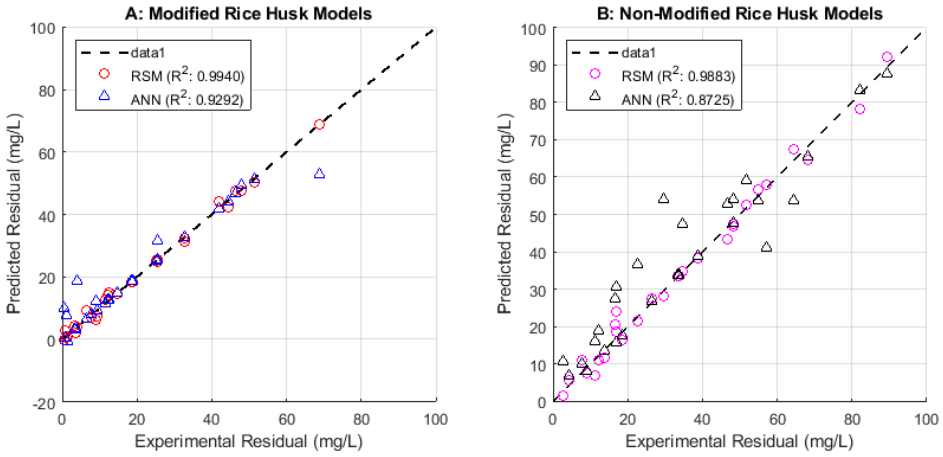

Figure 9: Parity plots for RSM and ANN predictions.

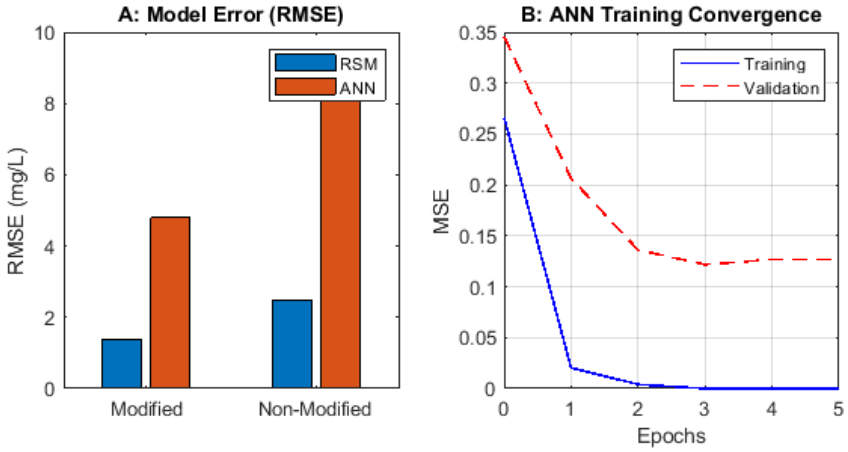

Figure 10: Model errors and ANN training convergence.

3.10. Comparison with recent Cr (VI) treatment studies

Table 9 benchmarks the present results against recent agricultural adsorbents and conventional treatment approaches. The maximum removal of 98.2% is comparable to several high-performing biochars and activated carbons. However, direct ranking by percentage removal is inappropriate because studies differ in influent concentration, dose, contact time, matrix composition and analytical method. Conventional membrane, ion-exchange and electrochemical systems can achieve very low final concentrations or faster treatment, but they require manufactured media, pressure, electrical energy, catalysts or management of regeneration streams and precipitated solids.

Table 9: Benchmark against recent Cr(VI) treatment studies.

Material/technology	**Representative conditions**	**Reported performance**	**Engineering comparison**	**Source**
Nitric-acid-modified rice husk (present study)	20-100 mg/L; pH 2-10; 0.10-1.00 g; 10-70 min	Maximum 98.2%; mean 67.0%	Low-cost feedstock; acid washing and spent-sorbent control required	Present study
Rice-husk biochar	pH 5.2; equilibrium about 2 h	96.8%; capacity 195.24 mg/g	High capacity; pyrolysis energy and longer contact time	Khalil *et al.* (2020)
Amide-modified rice-husk biochar	pH 2; 100 mg/L; 2 g/L; 60-120 min	97%; capacity 215.42 mg/g	Strong performance; additional functionalization chemistry	Ali *et al.* (2023)
MgO-rice-husk-ash composite	Mining wastewater; batch adsorption	Up to 79.2% Cr(VI)	Real-matrix relevance; nanoparticle synthesis adds cost	Mustapha *et al.* (2024)
Activated carbon from water hyacinth	2.25 mg/L; pH 5; 2 g; 90 min	98.4%	High surface area; lower influent concentration and activation demand	Fito *et al.* (2023)
Magnetic ion-exchange resin	Optimized batch conditions	Capacity 197 mg/g	Regenerable and separable; synthetic resin cost and brine waste	Ren *et al.* (2020)
Silk/polyamidoamine membrane	Static and flow tests, 1-10 mg/L	Final Cr(VI) below 50 µg/L under selected flow tests	Polishing to low concentration; membrane fabrication and regeneration	Ferruti *et al.* (2023)
Flow-by porous graphite electrode	50 mg/L; pH 2; 2.25 mA/cm²; 0.278 mL/s; 10 min	99.97% Cr(VI) removal	Fast and controllable; electrical demand and electrode management	Kamel and Bastaweesy (2024)
Palladized membrane biofilm reactor	1000 µg/L Cr(VI); H_2-driven reduction	>99% reduction; total Cr <50 µg/L	Very low effluent concentration; catalyst, H_2 supply and reactor complexity	Wu *et al.* (2024)

The benchmark indicates that modified rice husk is most defensible as a low-cost primary or intermediate adsorption step rather than a proven polishing technology. Its practical advantage is local feedstock availability, while its principal disadvantages are acid consumption, wash-water generation, uncertain regeneration performance and the need to verify oxidation-state-specific chromium removal in real wastewater.

3.11. Practical implications, scalability and limitations

Scale-up should proceed from batch screening to fixed-bed columns using real electroplating or tannery wastewater. Competing sulphate, chloride, nitrate, phosphate, dissolved organic matter and suspended solids may reduce capacity or alter chromium speciation. Process design must therefore include influent equalization, pH control, hydraulic loading, breakthrough behavior and a polishing step where stringent discharge limits apply. Economic feasibility depends not only on the nominally low cost of rice husk but also on carbonization energy, HNO_3 consumption, neutralization and washing water, drying, labour, transport and disposal or recovery of chromium-loaded solids. Regeneration/desorption cycles, sorbent attrition and chromium leaching should be tested before claiming reuse. The current study is limited by synthetic single-solute water, three replicated centre points only, no direct Cr(VI)/Cr(III) speciation, no BET or pH-point-of-zero-charge measurement, no regeneration or column data and semiquantitative EDS without chromium confirmation. These limitations define the next validation steps rather than negating the observed comparative benefit of modification.

4.0 CONCLUSIONS

Nitric-acid modification substantially improved rice-husk treatment performance across the 29-run design. Modified rice husk achieved 67.00% mean removal and 98.2% maximum removal, compared with 45.66% and 86.0% for the non-modified material. pH was the dominant factor, and the strong concentration-pH interaction showed that acidity becomes increasingly important as influent concentration changes. The quadratic RSM provided the best performance for this small dataset and remained robust under LOOCV (R^2cv = 0.9701 for modified and 0.9393 for non-modified rice husk), although significant lack of fit and the boundary optimum require cautious interpolation. The model-based optimum occurred at pH 2.0, 100 mg/L, 1.00 g and 70 min. Compared with recent studies, the maximum removal is competitive, but practical deployment still requires oxidation-state-specific analysis, real-wastewater validation, regeneration, column testing, cost assessment and safe management of chromium-loaded adsorbent.

ACKNOWLEDGEMENTS

The authors acknowledge the Civil Engineering Laboratory, Michael Okpara University of Agriculture, Umudike, and the technical personnel who supported adsorbent preparation, instrumental analysis and data processing.

REFERENCES

Ali, A., Alharthi, S., Al-Shaalan, N.H., Naz, A. and Fan, H.-J.S. (2023). Efficient removal of hexavalent chromium (Cr(VI)) from wastewater using amide-modified biochar. Molecules, 28(13), 5146. https://doi.org/10.3390/molecules28135146

Bansal, M., Garg, U., Singh, D. and Garg, V.K. (2009). Removal of Cr(VI) from aqueous solutions using pre-consumer processing agricultural waste: A case study of rice husk. Journal of Hazardous Materials, 162, 312-320. https://doi.org/10.1016/j.jhazmat.2008.05.037

Farooque, K.N., Zaman, M., Halim, E., Islam, S., Hossain, M., Mollah, Y.A. and Mahmood, A.J. (2009). Characterization and utilization of rice husk ash from rice mills of Bangladesh. Bangladesh Journal of Scientific and Industrial Research, 44(2), 157-162.

Ferruti, P., Alongi, J., Barabani, E., Manfredi, A. and Ranucci, E. (2023). Silk/polyamidoamine membranes for removing chromium VI from water. Polymers, 15(8), 1871. https://doi.org/10.3390/polym15081871

Fito, J., Tibebu, S. and Nkambule, T.T.I. (2023). Optimization of Cr(VI) removal from aqueous solution with activated carbon derived from Eichhornia crassipes under response surface methodology. BMC Chemistry, 17, 4. https://doi.org/10.1186/s13065-023-00913-6

Kamel, M.M. and Bastaweesy, A.M. (2024). Removal of chromium ions (Cr6+) and nickel ions (Ni2+) from simulated industrial wastewater using flow-by-porous electrode. Water, Air, & Soil Pollution, 235, 480. https://doi.org/10.1007/s11270-024-07246-7

Khalil, U., Shakoor, M.B., Ali, S., Rizwan, M., Alyemeni, M.N. and Wijaya, L. (2020). Adsorption-reduction performance of tea waste and rice husk biochars for Cr(VI) elimination from wastewater. Journal of Saudi Chemical Society, 24(11), 799-810. https://doi.org/10.1016/j.jscs.2020.07.001

Liu, H., Yao, R., Yu, M., Ye, Z., Lu, Y., Yu, X., Tang, J. and Sun, J. (2025). Converting waste into treasure: Efficient adsorption of Cr(VI) using iron-modified rice straw biochar. Toxics, 13(6), 458. https://doi.org/10.3390/toxics13060458

Mahmoud, A.S., Mohamed, N.Y., Mostafa, M.K. and Mahmoud, M.S. (2021). Effective chromium adsorption from aqueous solutions and tannery wastewater using bimetallic Fe/Cu nanoparticles: Response surface methodology and artificial neural network. Air, Soil and Water Research, 14, 11786221211028162. https://doi.org/10.1177/11786221211028162

Moussavi, G. and Barikbin, B. (2010). Biosorption of chromium(VI) from industrial wastewater onto pistachio hull waste biomass. Chemical Engineering Journal, 162, 893-900. https://doi.org/10.1016/j.cej.2010.06.032

Mustapha, L.S., Jacob-Oricha, S.O., Yahya, M.D., Lau, S.Y., Yusuff, A.S. and Obayomi, K.S. (2024). Effective removal of Cr(VI) and Pb(II) ions from mining wastewater using eco-friendly synthesized magnesium oxide nanoparticles incorporated rice husk ash. Environmental Advances, 15, 100507. https://doi.org/10.1016/j.envadv.2024.100507

Ngah, W.S.W. and Hanafiah, M.A.K.M. (2008). Removal of heavy metal ions from wastewater by chemically modified plant wastes as adsorbents: A review. Bioresource Technology, 99, 3935-3948. https://doi.org/10.1016/j.biortech.2007.06.011

Ozioko, H.O. and Eze, E.E. (2025). Predictive modeling of CBR and compressibility in lime-stabilized lateritic soil using machine learning and PCHIP data augmentation. Discover Civil Engineering, 2, 141. https://doi.org/10.1007/s44290-025-00304-x

Ren, Y., Han, Y., Lei, X., Lu, C., Liu, J., Zhang, G., Zhang, B. and Zhang, Q. (2020). A magnetic ion exchange resin with high efficiency of removing Cr(VI). Colloids and Surfaces A: Physicochemical and Engineering Aspects, 604, 125279. https://doi.org/10.1016/j.colsurfa.2020.125279

Ren, Z., Li, Z., Tang, H., Yang, L., Zhu, J. and Jing, Q. (2025). Analysis of response surface and artificial neural network for Cr(VI) removal column experiment. Water, 17(8), 1211. https://doi.org/10.3390/w17081211

Vinayagam, R., Dave, N., Varadavenkatesan, T., Rajamohan, N., Sillanpää, M., Nadda, A.K., Govarthanan, M. and Selvaraj, R. (2022). Artificial neural network and statistical modelling of biosorptive removal of hexavalent chromium using macroalgal spent biomass. Chemosphere, 296, 133965. https://doi.org/10.1016/j.chemosphere.2022.133965

Wu, C., Zhou, J., Pang, S., Yang, L., Lichtfouse, E., Liu, H., Xia, S. and Rittmann, B.E. (2024). Reduction and precipitation of chromium(VI) using a palladized membrane biofilm reactor. Water Research, 249, 120878. https://doi.org/10.1016/j.watres.2023.120878